Journal of
Composites Science

MDPI

Article

Assessment of the Attenuation Properties of Commercial Lead-Free Radiation-Shielding Composite Materials Against Medical X-rays

Anka Trajkovska Petkoska

Faculty of Technology and Technical Sciences, St. Kliment Ohridski University-Bitola, Dimitar Vlahov, 1400 Veles, North Macedonia; anka.trajkovska@uklo.edu.mk

Abstract: Six commercial, lead-free, radiation protective materials were tested for their attenuation across a range of X-ray energies used in medical diagnostic imaging and interventional radiology. While all the tested materials showed the specified attenuation at the X-ray energy claimed by their manufacturers, only two of the materials showed satisfactory attenuation in an extended range of medical X-ray energies (generated in X-ray tubes with voltages between 50 and 150 kV). The lead-free materials are lighter than the lead-containing materials, which is very important for those wearing the radiation protective garments for an extended time; however, the main focus in the promotion of radiation-shielding materials should still be on their attenuation efficacy against both the primary and the scattered X-rays present in medical environments. The end users should be informed on the material attenuation in an extended energy range, especially in the range where scatter radiation occurs, and not just about the peak material attenuation performance at energies where the X-rays are generated. Scatter radiation is the main reason for the occupational radiation exposure of medical personnel, who should have the whole picture about the shielding ability of the protective garments that they strongly rely on.

Keywords: X-rays; primary radiation; scatter radiation; metal-filled elastomers; lead-free composites

Citation: Trajkovska Petkoska, A. Assessment of the Attenuation Properties of Commercial Lead-Free Radiation-Shielding Composite Materials Against Medical X-rays. *J. Compos. Sci.* **2023**, *7*, 424. https://doi.org/10.3390/jcs7100424

Academic Editor: Francesco Tornabene

Received: 7 September 2023
Revised: 26 September 2023
Accepted: 7 October 2023
Published: 9 October 2023

1. Introduction

Human exposure to different ionizing radiation rays is becoming more frequent due to the extensive use of ionizing rays, such as X-rays, in medical diagnostic imaging, interventional radiology, radiation therapy, nuclear medicine, and other applications. Medical imaging, which enables a visual representation of different tissues and organs of the human body and is widely used to distinguish normal and abnormal anatomy and physiology of the body, has become a foundation for diagnosis and therapy in numerous diseases. In interventional radiology, the physician not only interprets the medical images, but also uses imaging to guide surgical interventions that diagnose, treat, and cure many kinds of health conditions. Many traditional surgical procedures are becoming more precise and minimally invasive procedures thanks to the advanced imaging techniques using X-rays [1–5]. Due to the ionizing nature, the commonly used X-rays in medicine are harmful for those exposed to them. For example, it is known that the exposure to ionizing radiation has many adverse health effects, such as increased risks of cancers and deadly acute radiation syndrome (fatigue and loss of appetite), among others. Moreover, X-rays are potentially harmful not only for the patient, but also for the interventional radiologists and operators during the interventional imaging methods, such as fluoroscopy and computed tomography (CT). The complexity of the radiation exposure conditions during imaging and interventional practices makes the radiation protection of the exposed workers a challenging task. For instance, one of the biggest challenges in radiation protection is not only the protection from primary X-ray beams, but also protection from secondary, or so-called scatter, radiation [6–10]. *Primary radiation* is related to the X-rays generated from the X-ray tube. *Secondary radiation*

is the X-ray radiation that is created when the primary beam encounters any solid matter, e.g., the patient, X-ray table, or protective clothing, resulting in a portion of the X-rays being absorbed and a portion being deflected in different direction(s) as secondary X-rays. Scatter X-ray radiation is a form of secondary radiation, where the X-ray is deflected from the incident direction in a different direction, usually accompanied by a loss in energy due to the collisions between the X-ray photons and the orbital electrons of atoms, which are in the path of the X-rays [7]. The scatter radiation is not easily predicted and, thus, cannot be easily controlled. Unwanted exposure to anyone around the X-ray source is possible, besides the fact that the scattered rays have much less energy than the incident X-rays. *Tertiary radiation* is caused as the scattered X-rays are deflected from the walls, floor, ceiling, and surrounding air, and is characterized by much lower energy than the secondary X-rays [8]. Therefore, it is of crucial importance to have adequate radiation protection for the patients and the medical staff, *viz.* radiographers, intervention operators, and others, in medical settings where X-rays are used. In order to provide efficient radiation shielding, the phenomena occurring in the protective materials as the X-ray photons are passing through the material, as well as their probability of happening, should be understood. As the X-rays are travelling throughout the material, they interact with the atoms of the shielding material and are either absorbed or scattered [3,11]. The X-ray scattering depends on several effects, among which the most common that occur in the shielding material are [3,11]:

Coherent (elastic) scattering occurs when the incident X-rays change their direction upon interaction with the outer electrons of the atoms in the shielding material, but still remain with the same energy. This elastic scattering is dependent on the metal atomic number, Z, and usually occurs at X-ray photon energies of less than 10 keV.
Photoelectric effect occurs when the X-rays are colliding with an electron closer to the nucleus in the atoms of the shielding material, the electron is being ejected from its shell, and then its "spot" is filled with an electron from an outer shell, a process that is accompanied by an emission of fluorescent X-rays characteristic for that element. The fluorescent X-rays are usually of lower photon energy than the incident X-rays and are highly dependent on the Z-number of the element(s) in the shielding material.
Compton effect occurs when the incident X-rays are deflected from their original direction by the loosely bound outer electrons of the atoms in the shielding material, which is associated with a partial loss of the incident photon energy. The photons continue to move throughout the material in a different direction with diminished energy until they undergo other interactions or leave the medium at a different angle than the incident X-rays. The energy shift depends mostly on the angle of scattering and not on the nature of the material. This is a type of incoherent scattering since the X-ray photon energy change is not always orderly and is not consistent; therefore, it is hard to predict. The probability for the Compton effect is directly proportional to the electron density and the physical density of the material, but does not depend on the Z-number, unlike the photoelectron effect.

In general, the photoelectric effects are dominant for photon energies below 30 keV, while the Compton effects are more pronounced for energies above 30 keV.

There are a few other effects that can occur as the X-ray photons are passing through the shielding material and are highly dependent on the energy of the incident photons; however, in the range of radiological X-ray energies, the two key interaction processes are the photoelectric and the Compton effect. The so-called scatter radiation (which is mainly due to the Compton effect) is the principal source of occupational exposure to radiographers, doctors, operators, and other medical personnel.

Lead (Pb) has been a material of choice for radiation protection for a long time due to its highly efficient interactions with the incident X-ray photons across a broad range of X-ray energies, thus, significantly enhancing the attenuation capabilities of the lead-containing materials, along with its economical availability. However, the toxicity of Pb has raised serious concerns, as excessive exposure to Pb potentially leads to increased blood pressure, nerve conditions, fatigue, drowsiness, fertility disorders, and so on, in addition to causing

back strain and other orthopedic issues for those who wear heavy Pb-protective garments for extended periods of time. Furthermore, Pb used in the modern protective garments contains the natural nucleotide ^{210}Pb and its daughter ^{210}Bi, which belongs to the uranium series—their radiation has been proven, although very low. Moreover, Pb is treated as hazardous waste for disposal due to its negative impacts on the environment [11,12].

To overcome all these concerns, lead-free protective materials have been proposed and introduced in the radiation protection industry as lighter-weight and non-toxic materials [11,13–37]. Lead-free composite materials containing radiation-shielding metals, such as bismuth (Bi) [38–47], barium (Ba) [47–50], tungsten (W) [51–57], antimony (Sb) [58], tin (Sn) [59], and others, dispersed in a polymer matrix, usually provide X-ray protection in a narrower range of photon energies than Pb, which depends on their atomic Z-number and K-absorption edge [11,13]. Different composite material structures and protective garment designs, where the shielding metals are arranged into a single-layer, bilayer, or multi-layer structure, have been proposed for efficient shielding against scatter and primary X-rays [24–28,60,61]. Some of the composite designs include more than one non-lead metal in a form of micrometer- and/or nano-sized particles dispersed in an elastomeric polymer matrix, [38–42,51–54]. Moreover, radiation-shielding fibers, yarns, and textiles, manufactured by different methods, such as coating, impregnation, and so on, have been proposed [62–71]. Additional benefits, such as no environmental concerns for their disposal and the potential of materials' recyclability, have been associated with the use of lead-free radiation protective garments.

During earlier years of lead-free materials' development, it was not adequately recognized that lead-free materials exposed to diagnostic X-ray photons could produce characteristic X-ray emissions yielding scatter X-rays (photoelectric effect) [72,73]. Since this scatter radiation is able to leave the shielding material at different angles than the incident beam, the shielding capability of lead-free materials is usually lower than that of Pb. This is particularly critical for lead-free protective materials consisting of metals with medium atomic Z-numbers, as in these materials, a significant amount of characteristic X-ray emission occurs at typical diagnostic X-ray energies of 30–80 keV. For comparison, in Pb-containing materials, no fluorescence radiation occurs below 80 keV, and therefore, this was not an issue with Pb-shielding materials. Eder et al. identified that the fluorescence of lead-free materials is the main reason for their reduced shielding capability compared to Pb-containing materials [72].

To date, lead-free radiation protective materials have been mainly promoted and offered to end users according to their lead equivalence, LEV, expressed in millimeters Pb (mmPb). The measurement of LEV is performed in a well-defined X-ray beam geometry, narrow-beam geometry (NBG), or broad-beam geometry (BBG), according to certain standards, such as the IEC 61331-3:2014 [74]. The conventional LEV of a sheet of radiation protection material (PM) is actually the thickness of lead (mmPb) that would result in the same reduction of air kerma as Pb in a narrow-beam configuration. The NBG measures only the attenuation of the primary X-ray beam by the shielding material, which is usually performed in a geometry where the test sample of protective material is placed at a large distance from the small detector, while the secondary (scatter) radiation, which exits the material at different angles than the incident primary beam, is missed. In order to correct this shortcoming for lead-free PMs, some of the standards including IEC have been modified with the BBG test setup, where the tested shielding material specimen is placed closer to a larger detector to capture the effects of the scatter radiation, in addition to those of the primary X-rays, as they are passing through the PM. Consequently, the attenuation of lead-free materials measured in BBG is usually lower compared to that measured in NBG. However, BBG is a much more realistic test method for lead-free materials and should be used for testing and comparison of different lead-free PMs offered by different manufacturers. Furthermore, modifications of BBG have been suggested by the leading experts in the field in order to more reliably capture the shielding efficacy of lead-free PMs [74]. The modifications (IBG, BBG*) have been directed mainly towards exposure of a larger area

of the tested shielding material to the X-rays, which is located closer to the measuring air kerma detector, and thus, the scatter rays leaving the PM at different angles will contribute to the detector signal. As the PMs have been promoted to end users according to their LEVs, it is important to point out that the LEV, i.e., the protection level of lead-free PM, is a strong function of the test beam quality and geometry [75–79]. LEV reported at a single kV energy (usually a peak LEV for a given lead-free PM) is totally inadequate, as the amount of protection provided by such material at other X-ray photon energies is unknown.

The aim of this study is to compare the attenuation ability of different commercial lead-free radiation PMs across an extended range of X-ray energies, often used in medical radiology for diagnostic and interventional purposes (Table 1). For this purpose, six lead-free PMs used in personal protective garments, *viz*. aprons, vests, skirts, and thyroid shields, offered by different manufacturers, are assessed for their attenuation efficacy measured in the BBG* test setup [74].

Table 1. Typical tube X-ray voltages used in medical radiology.

Medicinal X-Rays	Tube Accelerating Voltage, kV
Mammography	20–30
Dental diagnostic	60–70
General diagnostic	40–140
Interventional radiology	60–120
Computed tomography (CT)	80–140

2. Materials and Methods

2.1. Materials

Six commercially available lead-free radiation-shielding aprons, offered by different manufacturers, were collected from several medical centers in the US and tested for their attenuation efficacy. The fabric outer layers of the aprons were removed, and the inside core radiation protective material (PM) sheets were cut into specimens adequate for analysis, such as qualitative imaging, and assessment of their mechanical and attenuation properties. All core PMs were labeled with an LEV of 0.25 mmPb by their manufacturers (note: the aprons have front panels with double-core PM sheets, each of 0.25 mmPb, with a total LEV of 0.50 mmPb).

2.2. Materials Characterization

The cross-section of the cut specimens of PMs were subjected to qualitative analysis with a scanning electron microscope (SEM, FEI Quanta 600 FEG) equipped with Energy-Dispersive X-ray (EDX) spectroscopy. According to the SEM/EDX images, which revealed double-layer (bilayer) and single-layer (monolayer) PM composite structures, the studied PMs with the bilayer structure were designated as PM-1b, PM-2b, PM-3b, and PM-4b, while those with a monolayer structure were designated as PM-5m and PM-6m. PMs tested in this study, along with the weights of 10×10 cm^2 PM specimens, are provided in Table 2.

Table 2. Weights of 10×10 cm^2 specimens of protective materials tested in this study, all specified with LEV 0.25 mm Pb.

Protective Material (PM)	Weight [g]
PM-1b	25.44
PM-2b	28.10
PM-3b	28.10
PM-4b	29.08
PM-5m	30.27
PM-6m	30.90
Lead-composite PM	33.30
Lead PM	36.30

The tensile strength and elongation until break of a dog-bone-shaped sample were tested with a universal testing machine (Instron® 4204 tensile testing instrument, Instron, Norwood, MA, USA) at a constant stretching rate of 500 mm/min at ambient temperature, while the tear strength was tested with Die-C-shaped specimens at the same stretching rate and ambient conditions.

The attenuation properties were assessed in both test geometries, NBG and BBG*, according to the IEC 61331-3:2014 in the Bavarian State Office of Weights and Measures (Munich, Germany) [74].

All of the radiation PMs' commercial names and manufacturers are not disclosed in this study, except the names and the manufacturer of PM-3b and PM-6m shielding materials (Strata 300 and Strata 500, respectively; Burlington Medical, LLC, Newport News, VA, USA) upon approval by the company to be disclosed in this study. The same manufacturer also provided aprons with lead-composite core PM and 100% lead core PM with an LEV of 0.25 mmPb, as well as PM-3b, PM-6m, lead-composite PM, and 100% lead PM with an LEV of 0.50 mmPb, which were used for comparative purposes only.

3. Results and Discussion

3.1. Qualitative Assessment

Over the past two decades, many attempts to develop lead-free X-ray-shielding materials have resulted in efficient and flexible commercial PMs with notable peak attenuation efficacies, usually measured at a single kV energy or in a narrow range of photon energies. Different PM structures with more than one non-lead metal have been successfully manufactured for efficient X-ray shielding, most of them having monolayer, bilayer, or multi-layer structure. In bilayer PMs, at least two different non-lead protective metals are distributed in two separate sublayers, while in the monolayer PMs, the non-lead metals are mixed together and dispersed in a single layer. The bilayer PM is usually used in such a way that the layer with the lower Z-metal is facing the X-ray source, while the layer with the higher Z-metal is placed close to the body, so that the scattering (fluorescence) caused by the low Z-metal is absorbed by the higher Z-metal behind it as the X-ray propagates throughout the shielding material. In this particular study, the bilayer materials, PM-1b, PM-2b, and PM-4b, are materials with a single physical layer comprising two sublayers, each containing different protective metal(s), while PM-3b is a material consisting of two physically separate layers (PM-3b,1 and PM-3b,2), each layer containing different protective metals put together in the protective apron. The monolayers, PM-5m and PM-6m, are materials with a physical single layer, where the X-ray-shielding metals are dispersed in a single layer and the on-going phenomena of X-ray absorption, photoelectric, and scattering effects occur simultaneously as the X-rays are passing through the PM layer.

Scanning electron microscope (SEM) images and the energy-dispersive X-ray spectroscopy (EDX) elemental maps of the cross-sections of representative composite PMs are shown in Figures 1 and 2. In particular, the SEM images, along with the EDS elemental maps of a cross-section of Sb-containing and Bi-containing sublayers of the bilayer PM-1b, are shown in Figure 1, while the SEM image and EDS elemental maps of a cross-section of a single composite layer PM-6m containing Sb- and Bi-particles are shown in Figure 2. A uniform dispersion of the metal particles in both types of PM structures has been observed, suggesting a potentially efficient radiation protection. Sb- and Bi-metal particles with sizes up to 100 μm and with wide particle size distribution ranges were detected in both types of PM structures. Additional EDS analysis (not shown in this study) revealed the presence of chlorine (Cl) in PM-1b, suggesting that the PM-1b elastomer matrix is most likely polyvinyl chloride (PVC), i.e., plastisol-based, while Cl was not observed in the EDS elemental map of PM-6m. The EDS imaging of the other PMs tested in this study reveal that PM-2b, PM-4b, and PM-5m also contain Cl, and most likely, all these materials are plastisol-based matrices, in which the metal particles are dispersed. The EDS elemental map of PM-3b, like the PM-6m, showed no presence of Cl, indicating a different elastomeric matrix used for dispersing the metal particles.

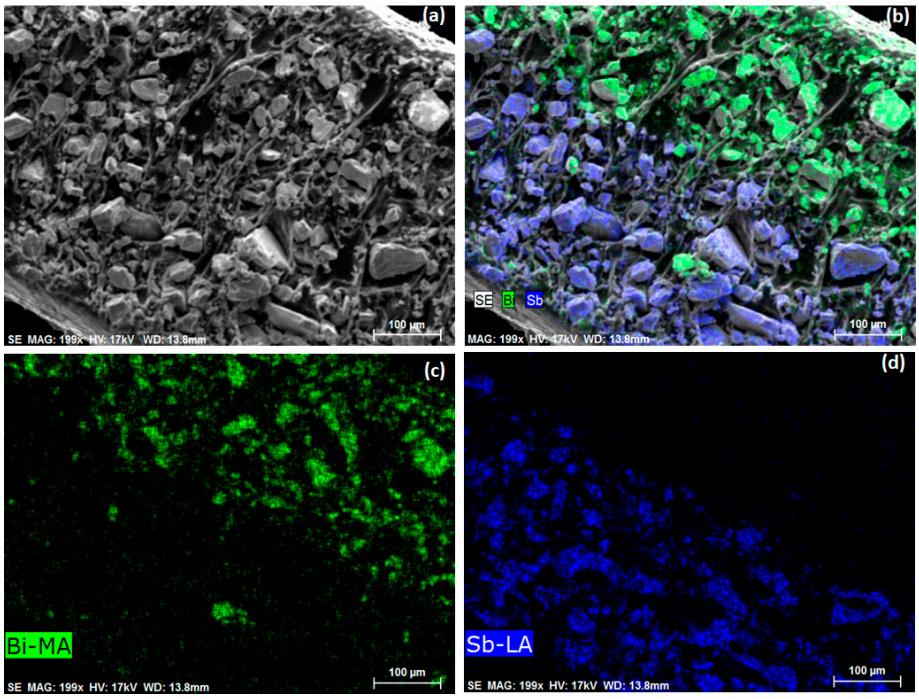

Figure 1. SEM images and EDX elemental maps of a cross-section of PM-1b. (**a**) SEM image of PM-1b cross-section. (**b**) SEM with EDX analysis of the PM-1b cross-section presented in (**a**). (**c**) Bismuth (Bi) elemental map of the PM-1b cross-section presented in (**a**,**b**). (**d**) Antimony (Sb) elemental map of the PM-1b cross-section presented in (**a**,**b**).

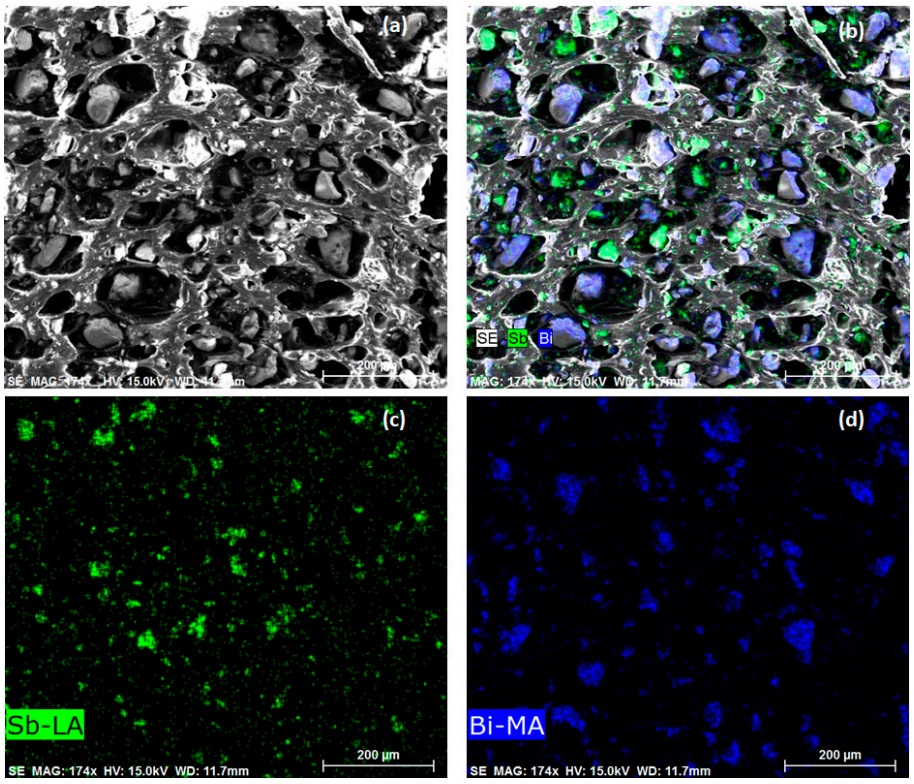

Figure 2. SEM images and EDX elemental maps of a cross-section of PM-6m. (**a**) SEM image of PM-6m cross-section. (**b**) SEM with EDX analysis of the PM-6m cross-section presented in (**a**). (**c**) Antimony (Sb) elemental map of the PM-6m cross-section presented in (**a**,**b**). (**d**) Bismuth (Bi) elemental map of the PM-6m cross-section presented in (**a**,**b**).

The bilayer composite material design, in general, could yield lighter-weight materials compared to the monolayer composite material designs. The weights of the tested materials are provided in Table 2 as weights taken of square specimens with sizes of 10 cm × 10 cm cut from the aprons' core radiation-shielding materials tested in this study. Indeed, the studied bilayer PMs are slightly lighter than the monolayer shielding materials. For example, the weights of the bilayer and the monolayer PM, PM-3b and PM-6m, respectively, manufactured by the same manufacturer using the same elastomer matrix and radiation-shielding metals, differ by ca. 9%, while the weights of the bilayer PM-2b and the monolayer PM-5m, both produced by the same manufacturer, again using the same elastomer and protective metals, differ by ca. 7%.

3.2. Mechanical Properties

The mechanical properties, such as tensile strength and elongation at break, and the tear strength of the materials tested are shown in Figure 3. It seems that the material structure, i.e., bilayer vs. monolayer structure, does not affect the tensile strength at break, the elongation at break, and the materials tear properties. What seems to be the determining factor in defining the tensile strength at break and the stretching of the material before it breaks is the nature of the elastomer matrix of the composite material, in which the radiation-shielding metals are dispersed. The PMs with a plastisol (PVC) matrix have an elongation at break of about 200%, while the PM-3b and PM-6m, which are most likely some type of a polyolefin-based elastomer, have a higher tensile strength at break and much greater elongation at break (Figure 3a).

As the area under the tensile strength–elongation curve relates to the toughness of the material, i.e., the ability of the material to absorb energy and deform without breaking, the non-plastisol materials tested in this study (PM-3b, PM-6m) have much higher toughness and can absorb much more deformational energy before they break compared to the plastisol-based materials (PM-1b, PM-2b, PM-4b, PM-5m). In fact, tough materials, like PM-3b and PM-6m, seem to have a good balance of ductility and strength.

The tear strength–elongation curves of all tested PMs are provided in Figure 3b. While some of the plastisol tested materials showed a slightly higher tear strength, the energy needed to tear the material is much greater for the non-plastisol materials (PM-3b, PM-6m) than for the plastisol-based PMs (PM-1b, PM-2b, PM-4b, PM-5m), as judged from the area under the tear strength–elongation curves.

The tear energy is actually a measure of the energy needed to tear the material from an initial stress point (like that present in Die-C-shaped specimens tested in this study) until the material completely fails. Polyolefin-based materials (PM-3b, PM-6m) need more energy to absorb before they tear apart than the plastisol ones. Again, the material structure, monolayer vs. bilayer, does not contribute to better mechanical properties within the same elastomeric material class. For instance, all plastisol-based materials, PM-1b, PM-2b, and PM-4b bilayer materials behaved similar in the tensile tests as the PM-5m monolayer material. PM-3b polyolefin bilayer, consisting of two physically separated Bi- and Sb-sublayers (PM-3b1 and PM-3b2), showed similar behavior as the polyolefin monolayer PM-6m. Therefore, the elastomeric material type was mainly responsible for the mechanical properties of tested PMs, such as the tensile strength and elongation at break, toughness, and tear energy.

Better toughness of the material usually means higher energy is needed for the materials to be torn apart, better resistance to external stresses, and, thus, better material durability, while more elongation of the material before it breaks is an indicator of higher resistance to kinks and breaks of the material.

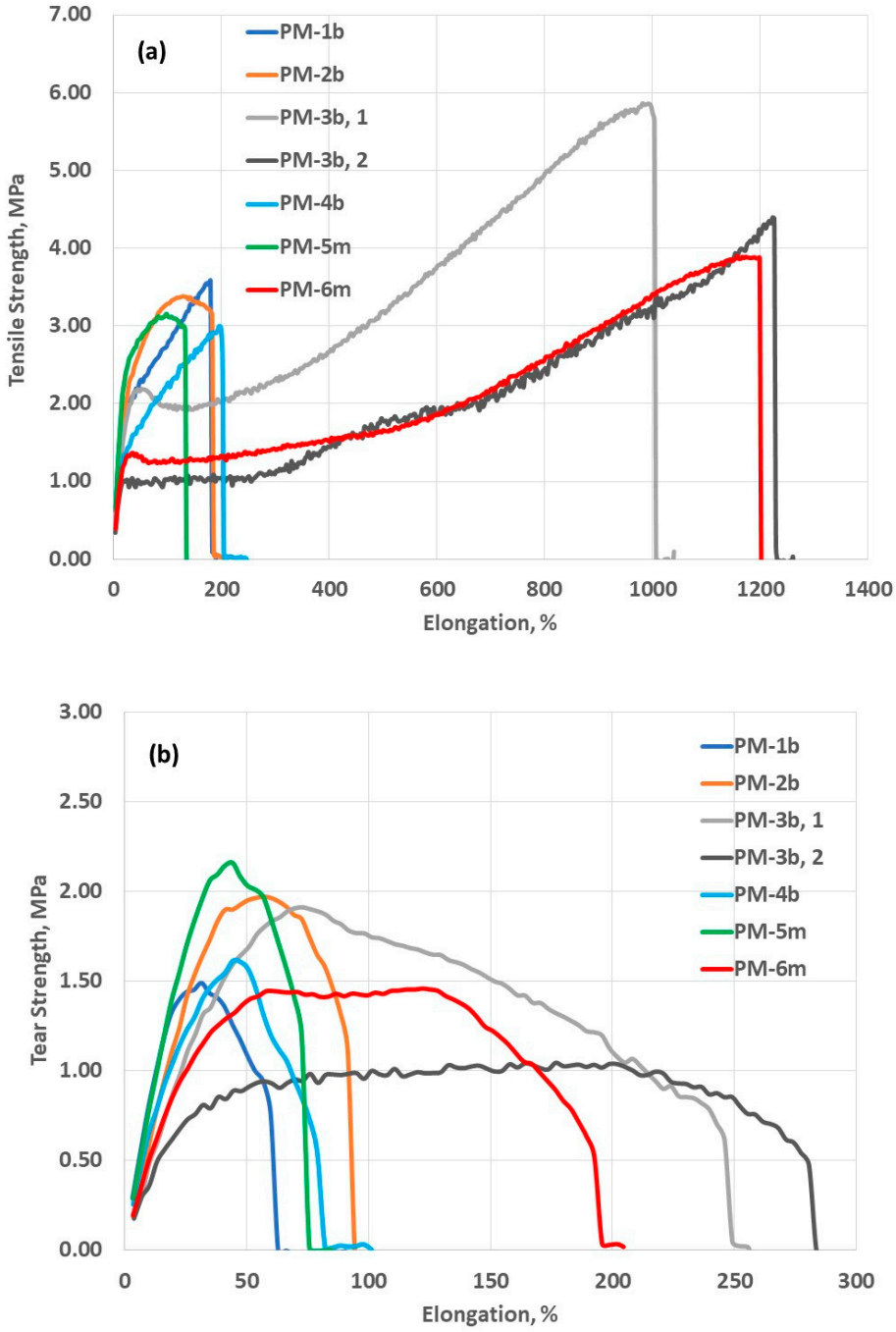

Figure 3. Mechanical properties of PMs tested in this study. (**a**) Tensile strength vs. elongation of PMs. (**b**) Tear strength vs. elongation of PMs.

3.3. Attenuation Properties

The attenuation properties of the PMs in this study were tested in two geometries, narrow-beam geometry, NBG, and modified broad-beam geometry, BBG*, as proposed by the international standard for protective garments IEC 61331-3:2014 [74]. The NBG mode was originally proposed to measure the attenuation of radiation protective materials exposed to a direct X-ray beam as the beam passes through the material. The BBG* test setup is more realistic for non-lead PMs, as it captures the scattering effects occurring during the propagation of the primary X-ray beam throughout the material. In the text below, the BBG* test results only will be discussed, as this study is assessing non-lead materials, and this test geometry is more reliable for such PMs. This is not the case with

lead-containing PMs, where the scattering effects are minimal, and therefore, the NBG test mode is sufficient.

The attenuation efficiency of PMs tested in this study, all designated with LEV 0.25 mmPb, and expressed as the attenuation percentage vs. the X-ray tube energy and as the percentage of the transmitted X-rays vs. the X-ray tube energy, is shown in Figure 4. The PM's attenuation efficacy was measured over a wide range of X-ray energies, generated in X-ray tubes with voltages from 50 kV to 150 kV, although the lead-free radiation PMs have been mainly recommended for use in medical environments that use X-ray tube voltages in a range from 60 kV to 110 kV. While a "good" protection of the tested lead-free PMs was not expected in the range greater than 110 kV of tube X-ray voltages, since this range is currently covered by the Pb-containing shielding materials, it was an objective of this study to assess the attenuation efficacy of the tested PMs at lower kV energies (below 60 kV). The PM's attenuation at lower kV energies is indicative of the shielding material's capability to protect against scatter X-rays, which are usually of lower energy than the primary X-rays and are generated as the primary X-rays are passing through the shielding material. As mentioned before, the main reason for the occupational radiation exposure of the medical operators is not the primary X-rays used for diagnosis or for interventional procedures, but the scatter X-rays present in different medical environments.

The attenuation properties of all materials tested in this study are presented in Figure 4a in the 50–150 kV range of X-ray tube accelerating voltages. The bilayer materials, along with the PM-6m monolayer, showed overall better performance than the PM-5m. While the bilayer structure did contribute to lighter-weight materials compared to the monolayer material designs, it did not result in significantly better attenuation properties among the PMs tested in this study. This is just the observation made for the presently tested six PMs, manufactured by different manufacturers, and collected at several medical centers in the US. The same observations can be made from the graphical presentations of % transmitted (leaked) X-rays through the tested PMs (Figure 4b). It is worth emphasizing here that improved attenuation properties of bilayer-based protective materials is, however, possible after further optimization of the material parameters, such as the metal filling ratio in the polymer matrix, the nature of protective metal (with respect to Z-number and K-absorption edge), metal particle sizes and particle size distributions in both sublayers of the bilayer structure, the material density, and so on. Therefore, the bilayer structure could yield lighter-weight and better attenuating materials if optimization of the relevant material's molecular parameters is adequately performed.

In the present study, the monolayer composite material, PM-6m, showed the best attenuation performance among the tested PMs, as can be seen from Figure 4c,d. This is an indication that, by optimization of the relevant material parameters, even a single-layer PM could yield to superior attenuation properties over a wide range of X-ray tube energies. Further optimization of the particle sizes and particle size distribution enabling efficient volume filling of the single-layer material could potentially yield additional weight reduction of the material.

As mentioned before, the scattered X-rays usually have lower energy than the primary X-rays, which are generated as the primary beam propagates throughout the shielding material and is deflected in different directions, mainly due to the photoelectric and Compton effects. Therefore, the attenuation ability of non-lead materials at lower kV energies is extremely important. The analysis of attenuation curves in the range of 50–110 kV of X-ray tube voltages (Figure 4c,d), which covers the lower kV range indicative of the scatter X-rays and extends across the kV range recommended for use of lead-free materials, revealed the attenuation ability of the studied PMs against both primary and scatter X-rays. The best attenuating PMs are PM-6m, PM-3b, and PM-4b, followed by PM-1b and PM-2b, while PM-5m did not provide the necessary protection in the low kV range. For instance, the percentage of the transmitted X-rays was around 1.09% for PM-3b and PM-6m for the X-rays generated with 50 kV X-ray tube voltage, 1.38% for PM-4b, 1.90% for PM-1b, 3.37% for PM-2b, and 7.28% for PM-5m. Although the percentages of X-rays that pass through

the tested materials seem to be similar for most of the tested materials, i.e., within 1–2% of that measured for PM-3b and PM-6m, except PM-5m, it should be noted that this can be significant information for the operators, who are exposed to both the leaked and the scattered radiation that has not been absorbed by the shielding material. For instance, PM-4b and PM-1b transmit 26% and 74% more X-rays at 50 kV than those transmitted through PM-3b and PM-6m, respectively, while PM-2b leaks more than 200% than the amount of X-rays leaked from PM-3b and PM-6m. Therefore, as new radiation protective materials are being developed and the focus has been directed towards light-weight lead-free materials, the responsible parties and the end users should pay more attention to the PM's ability to protect not only from primary, but also from scatter, radiation. The scatter radiation is minimal for lead, but for non-lead metals, the scattering effects can be up to 100% relative to the transmitted radiation due to the fluorescence, which is especially pronounced around the K-absorption edges for the non-lead metals that usually fall into the range of medical diagnostic X-rays.

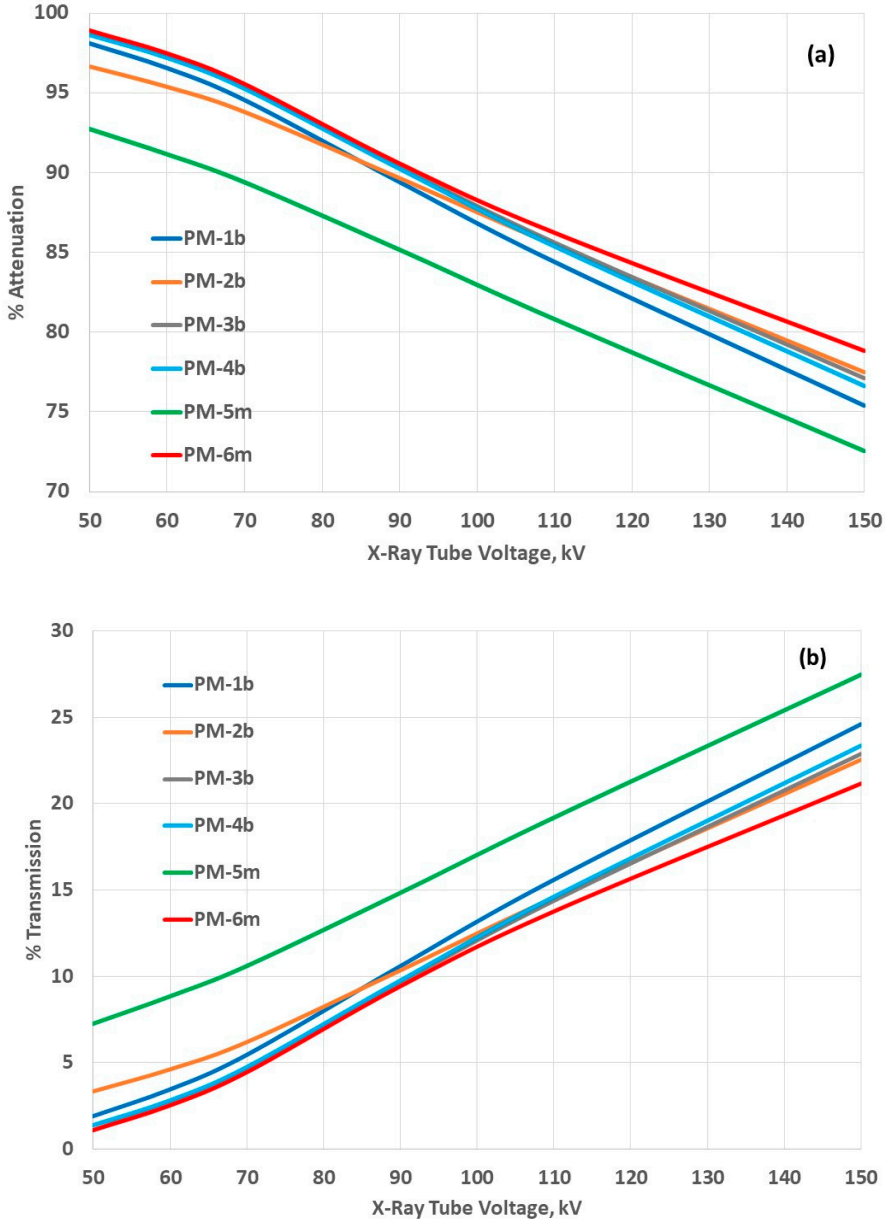

Figure 4. *Cont.*

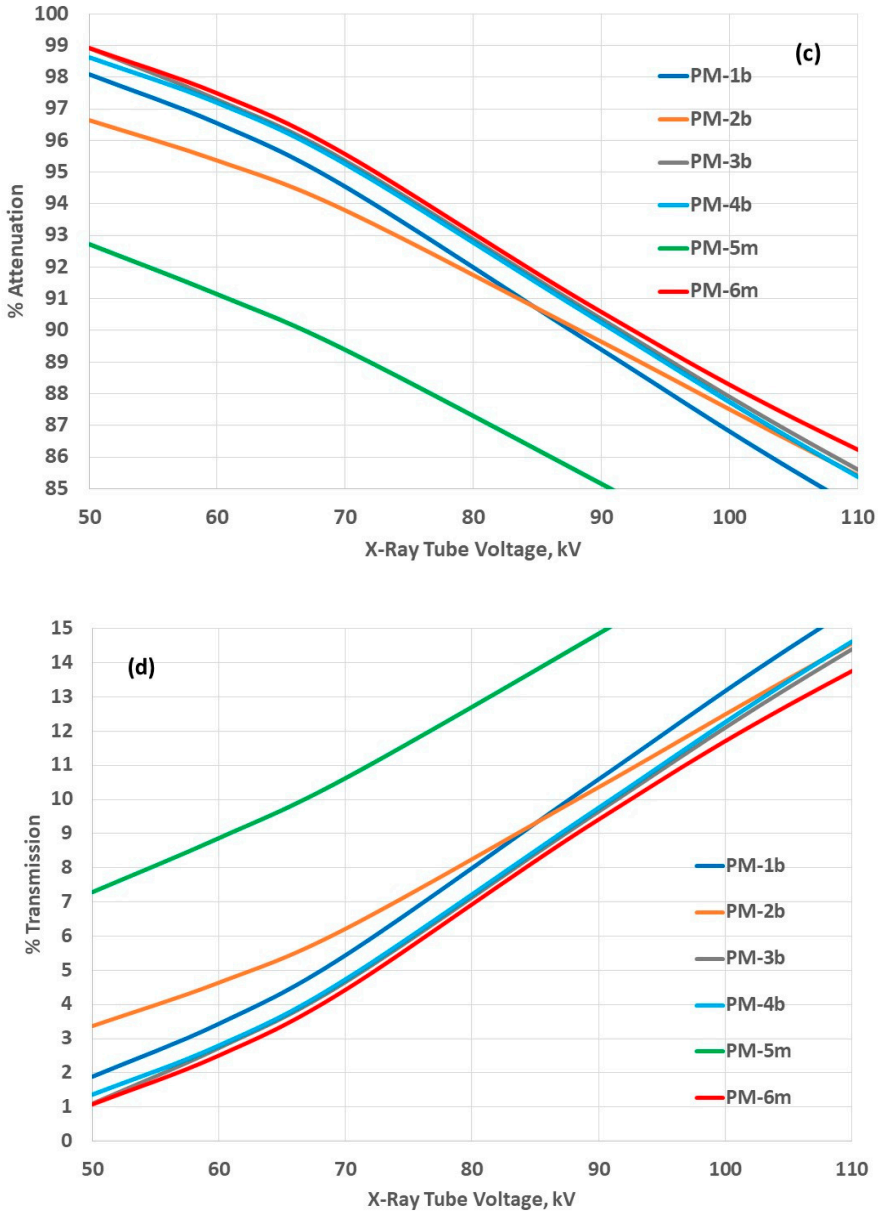

Figure 4. Attenuation properties for PMs tested in this study, all claimed to have an LEV of 0.25 mm Pb by their manufacturers. (**a**) Percentage X-ray attenuation in 50–150 kV range. (**b**) Percentage X-ray transmission in 50–150 kV range. (**c**) Percentage X-ray attenuation in 50–110 kV range. (**d**) Percentage X-ray transmission in 50–110 kV range.

For comparative purposes only, the attenuation of the tested lead-free composite materials was compared to that provided by lead-containing composite materials (Figure 5a). Lead-composite (Pb/Sb) material and 100% lead-containing PM, both with an LEV of 0.25 mmPb, the same as the lead-free PMs analyzed in this study, were tested for their attenuation efficacy in the same test geometry (BBG*). As expected, the studied lead-free materials differ the most in their protection efficacy from the lead-containing materials at higher kV energies, where actually lead-free materials are not recommended for use by the manufacturers. The attenuation percentage of three of the best attenuating lead-free materials in this study (PM-3b, PM-4b, PM-6m) was compared with that of lead-containing PMs in the lower kV range in Figure 5b. Less difference in the attenuation properties between lead-free and lead-containing materials was observed at lower kV (in the scatter range) than at higher kV. PM-6m showed the best performance when compared to the lead-containing PMs; while the leaked X-rays for PM-6m are around 1% at 50 kV, which

is the same level as that observed for the tested lead-containing PMs, the leaked X-rays for PM-6m are 13.76% at 110 kV compared to 13.07% and 12.70% for the lead- and lead-composite PMs, respectively (Figure 5c). PM-6m material attenuates the X-rays very well, similar to the attenuation observed for lead-composite and 100% lead-PMs.

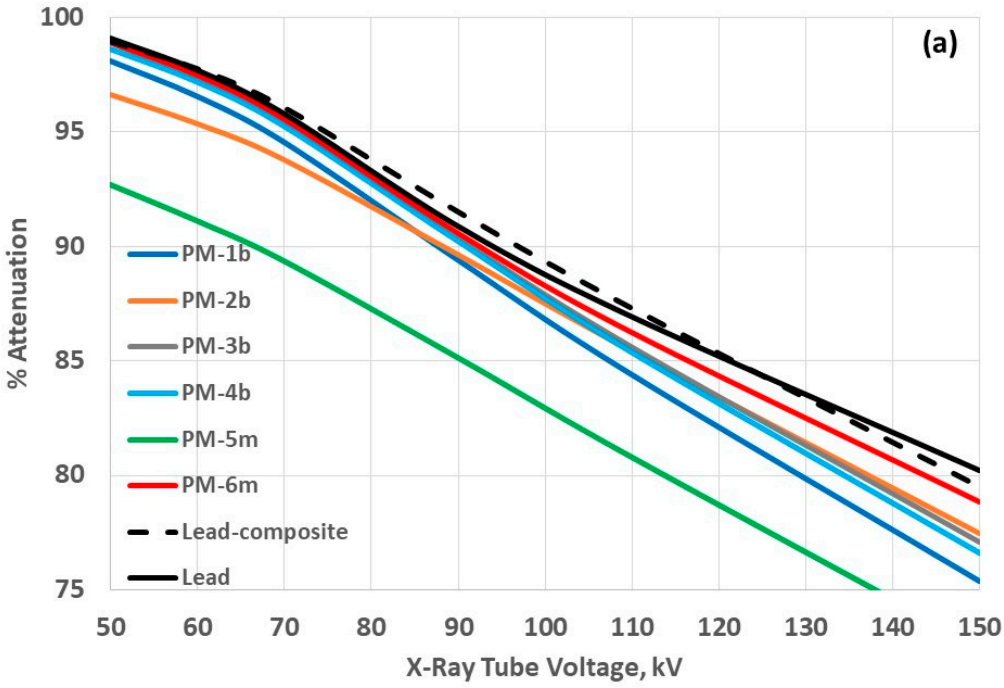

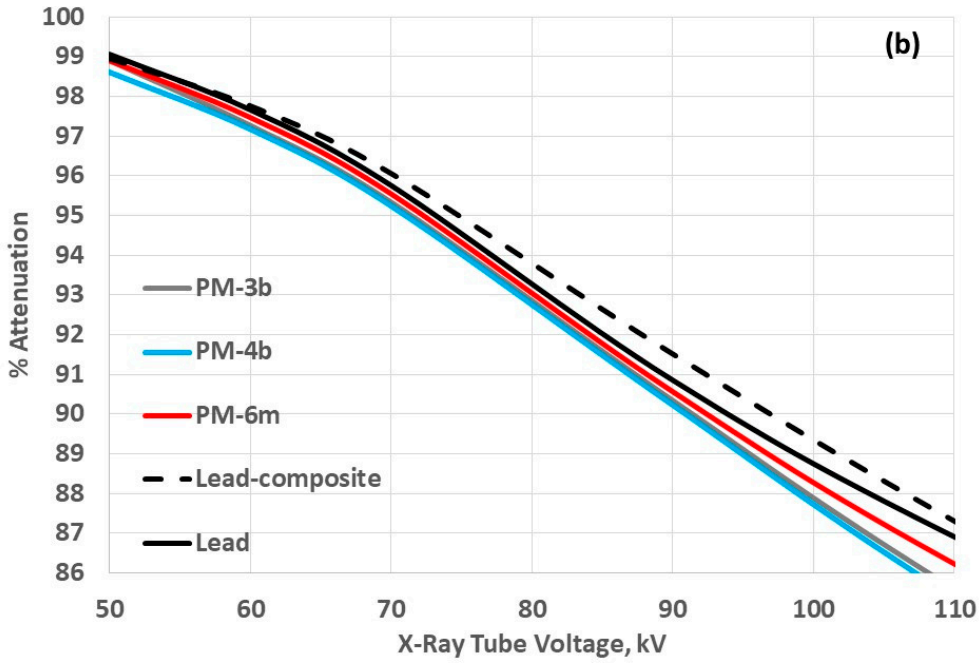

Figure 5. *Cont.*

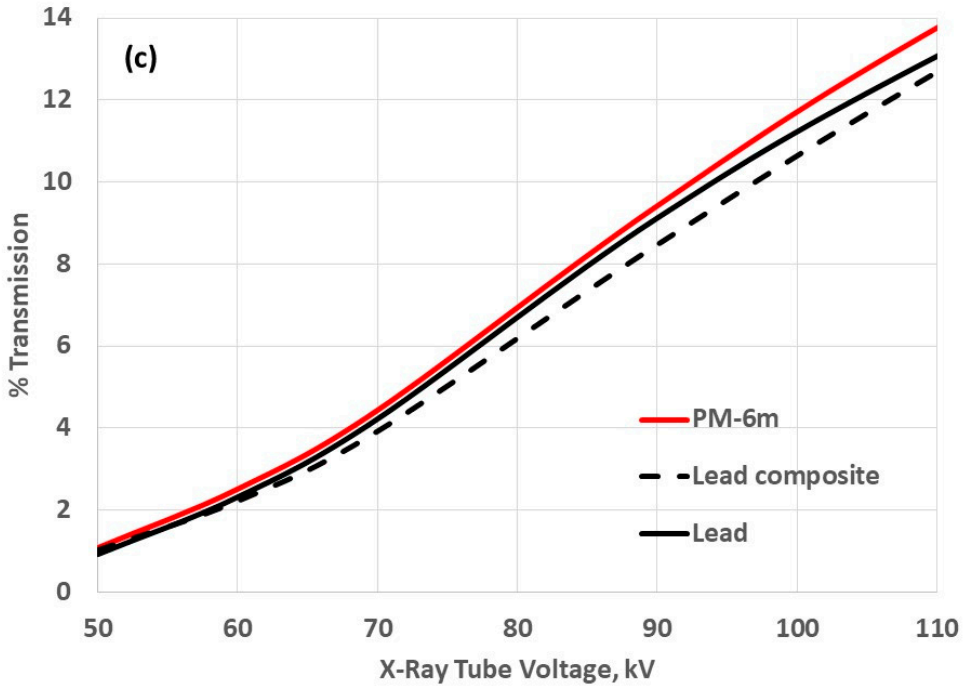

Figure 5. Comparison of the attenuation properties of PMs tested in this study with those of lead-composite and lead PMs, all claimed to have an LEV of 0.25 mm Pb by their manufacturers. (**a**) Comparison of the percentage X-ray attenuation of tested PMs with lead-containing PMs in 50–150 kV range. (**b**) Comparison of the percentage attenuation for three best performing PMs in this study with lead-containing PMs in 50–110 kV range. (**c**) Comparison of the percentage X-ray transmission for the best performing PM in this study with those for lead-containing PMs.

In instances when a higher protection level is required within the recommended range of use of lead-free PMs (X-rays generated in tubes with voltages between 60 and 110 kV), then PMs with a higher LEV could be used. For this purpose, one of the monolayer and one of the bilayer materials, PM-3b and PM-6m, with LEVs of 0.50 mmPb were tested, and their attenuation properties were compared with the PMs with 0.25 mmPb (Figure 6a,b). For comparison, 0.50 mmPb lead-containing PMs, manufactured by the same company as the PM-3b and PM-6m (Burlington Medical), were tested, too. It is obvious that the presented lead-free materials (PM-3b, PM-6m) indeed exhibit a protection level very close to that of lead-containing materials for both LEVs tested (0.25 mmPb and 0.50 mmPb) in this study and in the recommended range of their use (60–110 kV).

As the radiation protective aprons are being promoted and offered according to their LEV, the LEV values of the PMs analyzed in this study were extracted from their attenuation values measured in BBG* and are presented in Figure 7. The test method of how the LEV of a shielding material has been determined is very important, because this value strongly depends on the X-ray beam quality and X-ray energy. For instance, the LEV measured in NBG will be higher than the LEV measured in BBG* mode for the same material due to the scattered X-rays coming out of the lead-free PM and being missed in the NBG setup, but they are registered in the BBG* test setup and, thus, contribute to a lower LEV. All of the PMs studied here do satisfy the LEV claimed by the manufacturer at a single kV-energy (usually peak LEV value) or in the specific (usually narrower) kV range of X-ray energies. The test facility where all the PMs in this study were tested reports +/−7% uncertainty from the specified (nominal) LEV. After a careful analysis of the LEV values for all PMs tested and determined from the BBG* measurements (Figure 7), it is obvious that all the tested PMs do not satisfy an LEV of 0.25 mm Pb across a wider range of X-ray tube energies. All of the materials, except PM-3b and PM-6m, showed a consistently lower LEV at lower kVs than the manufacturers' specification of 0.25 mmPb, which is usually claimed for higher

kVs, where the X-rays are generated (usually 90 kV or 90–110 kV range). The blue-shaded area in Figure 7 presents the range of mmPb values that the tested PMs should have in order to pass the IEC standard (nominal LEV +/−7%) [74]. Only two of the tested materials, PM-3b and PM-6m, satisfied the IEC standard across the whole tested kV range from 50 kV to 150 kV.

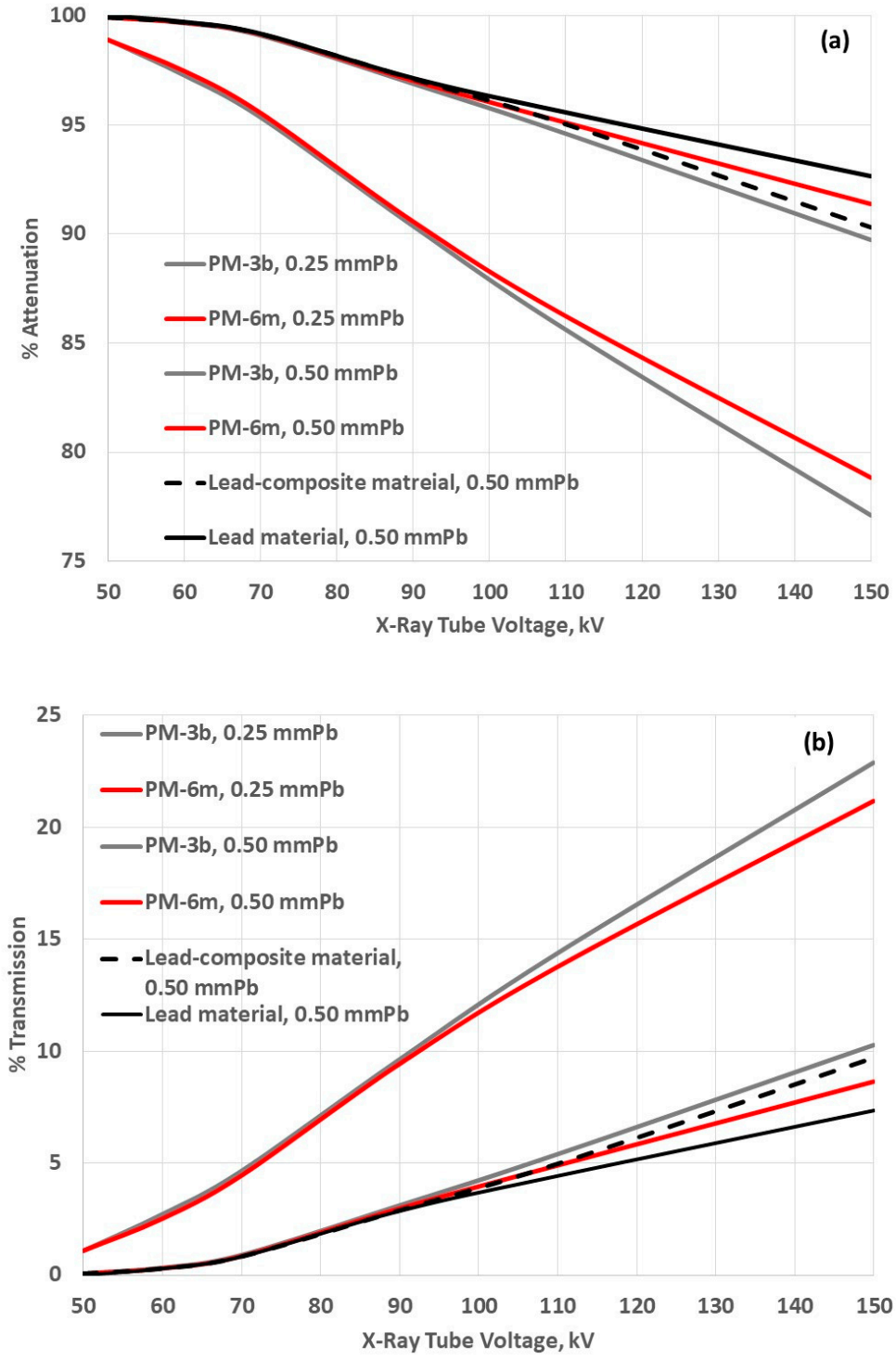

Figure 6. Comparison of the attenuation properties of two of the best performing PMs in this study with LEV of 0.25 mmPb with those of PMs with LEV of 0.50 mm. (**a**) Comparison of the percentage X-ray attenuation in 50–150 kV range. (**b**) Comparison of the percentage X-ray transmission in 50–150 kV range.

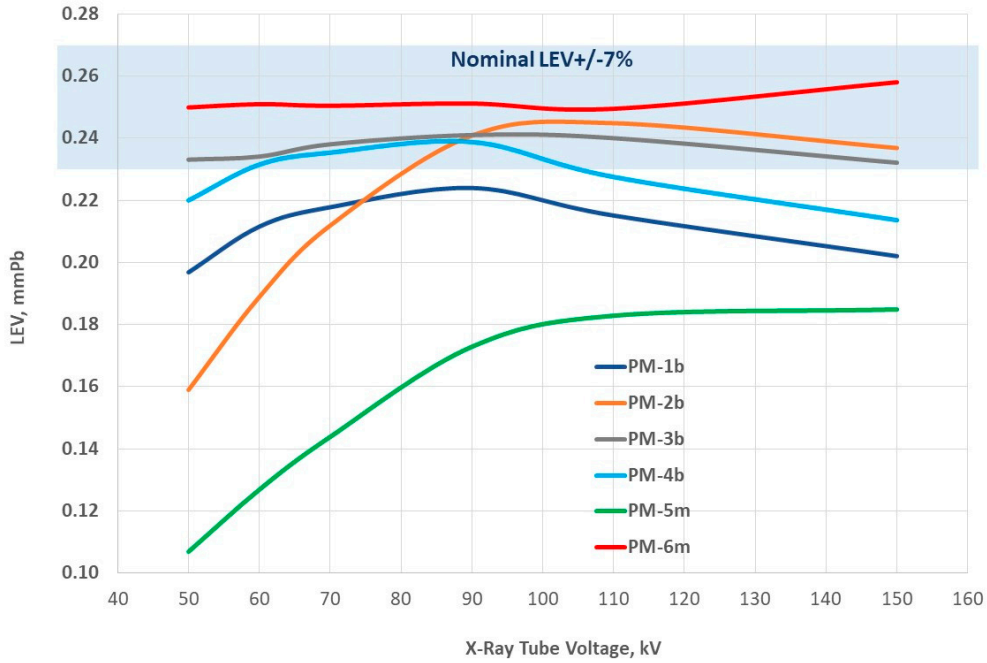

Figure 7. LEV of PMs tested in this study across 50–150 kV range, all claimed to have peak LEV of 0.25 mm Pb by their manufacturers. The shaded area means the nominal LEV value +/−7% uncertainty.

4. Conclusions

Six commercial radiation protective materials (PMs) manufactured by different manufacturers, all containing at least two radiation-shielding non-lead metals, were tested for their attenuation efficacy across a range of X-ray energies generated in X-ray tubes with voltages between 50 kV and 150 kV, often used in diagnostic medicine and interventional radiology. While all the tested materials showed the LEV of 0.25 mmPb at the X-ray energies claimed by their manufacturers, some of the materials showed a much lower LEV outside the specified range. Only two of the tested materials, the bilayer PM3-b and the monolayer PM6-m (Strata 300 and Strata 500, respectively, Burlington Medical, LLC, Newport News, VA, USA) showed a satisfactory and consistent LEV of 0.25 mm Pb +/−7% over the tested X-ray energy range. The lower attenuation (i.e., lower LEV) detected for some of the studied PMs was observed mostly at lower X-ray tube voltages (50–60 kV), which implies that these materials are not protective against the scatter X-rays generated as the primary X-rays are passing through the lead-free PMs, resulting in lower-energy scatter X-rays being deflected at different angles with respect to the incident X-rays. As occupational radiological exposure is mainly due to the scatter radiation, it is of vital importance for the radiation-shielding materials included in various personal protective garments to provide the necessary protection against both the scatter X-rays and the primary X-rays. The reported LEV by the manufacturers, usually as a peak LEV value at a single kV or for a narrow range of X-ray energies, is totally inadequate and puts the end users in dangerous situations for potential exposure to scatter X-ray radiation.

Overall, lead-free composite PMs can provide satisfactory attenuation across a range of medical X-ray energies, similar to that offered by lead-containing composite PMs, but at a reduced material weight. The weight reduction is a very important characteristic for those wearing the radiation protective garments for extended periods of time. In addition, lead-free materials offer other benefits, such as reduced (or no) toxicity, extended lifetime, and potential material recyclability. However, once again, the main focus in promotion of lead-free PMs should be on the PM's attenuation efficacy. Scatter radiation is a big concern for medical personnel, and the protective garments are being promoted to save lives; therefore, the PM should completely protect those who thoroughly rely on them. The

end users deserve to know about the protection level of the protective garments across an extended range of photon energies covering the primary and scatter X-rays, preferably measured in a BBG*, as the most relevant test method to access the protection level of lead-free PMs. Once the end users have the information of the PM's protection level against primary and scatter radiation, they can make an informed decision about what they would prefer for their own protection—a lighter-weight PM, or a PM with complete radiation protection.

Funding: This research received no external funding.

Data Availability Statement: Not applicable.

Conflicts of Interest: The author declares no conflict of interest.

References

1. Beyer, T.; Bailey, D.L.; Birk, U.J.; Buvat, I.; Catana, C.; Cheng, Z.; Fang, Q.; Giove, F.; Kuntner, C.; Laistler, E.; et al. Medical Physics and Imaging—A Timely Perspective. *Front. Phys.* **2021**, *9*, 634693. [CrossRef]
2. Hussain, S.; Mubeen, I.; Ullah, N.; Shah, S.S.U.D.; Khan, B.A.; Zahoor, M.; Ullah, R.; Khan, F.A.; Sultan, M.A. Modern Diagnostic Imaging Technique Applications and Risk Factors in the Medical Field: A Review. *Hindawi BioMed Res. Int.* **2022**, *2022*, 5164970. [CrossRef] [PubMed]
3. Berger, M.; Yang, Q.; Maier, A. X Ray Imaging. In *Medical Imaging Systems: An Introductory Guide*; Maier, A., Steidl, S., Horneggel, J., Eds.; Springer: Cham, Switzerland, 2018; pp. 119–145. [CrossRef]
4. Datta, A.; Zhong, Z.; Motakef, S. A new generation of direct X-ray detectors for medical and synchrotron imaging applications. *Sci. Rep.* **2020**, *10*, 20097. [CrossRef] [PubMed]
5. Kovács, A.; Bischoff, P.; Haddad, H.; Kovács, G.; Schaefer, A.; Zhou, W.; Pinkawa, M. Personalized Image-Guided Therapies for Local Malignencies: Interdisciplinary Options for Interventional Radiology and Interventional Radiotherapy. *Front. Oncol.* **2021**, *11*, 616058. [CrossRef] [PubMed]
6. Ferrari, P.; Ginjaume, M.; Hupe, O.; O'Connor, U.; Vanhavere, F.; Bakhanova, E.; Becker, F.; Campani, L.; Carinou, E.; Clairand, I.; et al. What Is Worth Knowing in Interventional Practices about Medical Staff Radiation Exposure Monitoring: A Review of Recent Outcomes of EURADOS Working Group 12. *Environments* **2022**, *9*, 53. [CrossRef]
7. Nowak, M.; Carbonez, P.; Krauss, M.; Verdun, F.R.; Damet, J. Characterisation and mapping of scattered radiation fields in interventional radiology theatres. *Sci. Rep.* **2020**, *10*, 18754. [CrossRef]
8. Eder, H.; Seidenbusch, M.; Oechler, L.S. Tertiary X-Radiation—A problem for Staff Protection? *Radiat. Prot. Dosim.* **2020**, *189*, 304–311. [CrossRef]
9. Pavlicek, W.; Sensakovic, W.F.; Zhou, Y.; Paden, R.G.; Panda, A.; Hines, J.; Naidu, S.G.; Oklu, R. Sample content of kinesthetic educational training: Reducing scattered X-ray exposures to interventional physician operators of fluoroscopy. *J. Appl. Clin. Med. Phys.* **2019**, *21*, 196–208. [CrossRef]
10. Khafaji, M.; Albadawi, G.H. Assessment of Scattered Dose to the Eye in Dentistry: A Systematic Review. *Cureus* **2023**, *15*, e43113. [CrossRef]
11. Low, I.M.; Azman, N.Z.N. *Polymer Composites and Nanocomposites for X-Rays Shielding*; Springer Nature Singapore Pte Ltd.: Singapore, 2020; ISBN 978-981-13-9809-4. [CrossRef]
12. Osanai, M.; Kudo, K.; Hosoda, M.; Tazoe, H.; Akata, N.; Kitajima, M.; Tsushima, M.; Komiya, N.; Kudo, M.; Tsujiguchi, T.; et al. The impact on the eye lens of radiation emitted by natural radionuclides (Lead-210) present in radiation protection glasses. *Radiat. Prot. Dosim.* **2019**, *188*, 13–21. [CrossRef]
13. Garg, T.; Shrigiriwar, A. Radiation Protection in Interventional Radiology. *Indian J. Radiol. Imaging* **2021**, *31*, 939–945. [CrossRef]
14. Shahzad, K.; Kausar, A.; Manzoor, S.; Rakha, S.A.; Uzair, A.; Sajid, M.; Arif, A.; Khan, A.F.; Diallo, A.; Ahmad, I. Views on Radiation Shielding Efficiency of Polymeric Composites/Nanocomposites and Multi-Layered Materials: Current State and Advancements. *Radiation* **2022**, *3*, 1–20. [CrossRef]
15. Li, Z.; Zhou, W.; Zhang, X.; Gao, Y.; Guo, S. High-efficiency, flexibility and lead-free X-ray shielding multilayered polymer composites: Layered structure design and shielding mechanism. *Sci. Rep.* **2021**, *11*, 4384. [CrossRef] [PubMed]
16. Asadpour, N.; Malekzadeh, R.; Rajabpour, S.; Refahi, S.; Mehnati, P.; Shanei, A. Shielding performance of multi-metal nanoparticle composites for diagnostic radiology: An MCNPX and Geant4 study. *Radiol. Phys. Technol.* **2022**, *16*, 57–68. [CrossRef] [PubMed]
17. More, C.V.; Alsayed, Z.; Badawi, M.S.; Thabet, A.A.; Pawar, P.P. Polymeric composite materials for radiation shielding: A review. *Environ. Chem. Lett.* **2021**, *19*, 2057–2090. [CrossRef] [PubMed]
18. Li, Q.; Wei, Q.; Zheng, W.; Zheng, Y.; Okosi, N.; Wang, Z.; Su, M. Enhanced Radiation Shielding with Conformal Light-Weight Nanoparticle–Polymer Composite. *ACS Appl. Mater. Interfaces* **2018**, *10*, 35510–35515. [CrossRef] [PubMed]
19. Kim, S.C.; Choi, J.R.; Jeon, B.K. Physical analysis of the shielding capacity for a lightweight apron designed for shielding low intensity scattering X-rays. *Sci. Rep.* **2016**, *6*, 27721. [CrossRef]

20. Almurayshid, M.; Alssalim, Y.; Aksouh, F.; Almsalam, R.; Alqahtani, M.; Sayyed, M.I.; Almasoud, F. Development of New Lead-Free Composite Materials as Potential Radiation Shields. *Materials* **2021**, *14*, 4957. [CrossRef]
21. Kim, S.-C. Comparison of Shielding Material Dispersion Characteristics and Shielding Efficiency for Manufacturing Medical X-ray Shielding Barriers. *Materials* **2022**, *15*, 6075. [CrossRef]
22. Eder, H.; Schlattl, H. Shielding effectiveness of X-ray protective garment. *Phys. Medica* **2021**, *82*, 343–350. [CrossRef]
23. Nambiar, S.; Osei, E.K.; Yeow, J.T.W. Polymer Nanocomposite-based Shielding Against Diagnostic X-rays. *J. Appl. Polym. Sci.* **2013**, *127*, 4939–4946. [CrossRef]
24. Thumwong, A.; Darachai, J.; Saenboonruang, K. Comparative X-ray Shielding Properties of Single-Layered and Multi-Layered Bi_2O_3/NR Composites: Simulation and Numerical Studies. *Polymers* **2022**, *14*, 1788. [CrossRef] [PubMed]
25. McCaffrey, J.P.; Mainegra-Hing, E.; Shen, H. Optimizing non-Pb radiation shielding materials using bilayers. *Med. Phys.* **2009**, *36*, 5586–5594. [CrossRef] [PubMed]
26. Gilys, L.; Griškonis, E.; Griškevičius, P.; Adlienė, D. Lead Free Multilayered Polymer Composites for Radiation Shielding. *Polymers* **2022**, *14*, 1696. [CrossRef] [PubMed]
27. Kim, Y.; Park, S.; Seo, Y. Enhanced X-ray Shielding Ability of Polymer–Nonleaded Metal Composites by Multilayer Structuring. *Ind. Eng. Chem. Res.* **2015**, *54*, 5968–5973. [CrossRef]
28. Park, S.; Kim, H.; Kim, Y.; Kim, E.; Seo, Y. Multilayer-Structured Non-leaded Metal/Polymer Composites for Enhanced X-ray Shielding. *MRS Adv.* **2018**, *3*, 1789–1797. [CrossRef]
29. Kazempour, M.; Saeedimoghadam, M.; Shooli, F.S.; Shokrpour, N. Assessment of the Radiation Attenuation Properties of Several Lead Free Composites by Monte Carlo Simulation. *J. Biomed. Phys. Eng.* **2015**, *5*, 67–76.
30. Nikeghbal, K.; Zamanian, Z.; Shahidi, S.; Spagnuolo, G.; Soltani, P. Designing and Fabricating Nano-Structured and Micro-Structured Radiation Shields for Protection against CBCT Exposure. *Materials* **2020**, *13*, 4371. [CrossRef]
31. Yücel, H.; Güllüoğlu, E.; Çubukçu, S.; Ali Üncü, Y. Measurement of the Attenuation Properties of the Protective Materials Used as a Thyroid Guard and Apron for Personnel Protection against Diagnostic Medical X-rays. *J. Phys. Sci.* **2016**, *27*, 111–128.
32. Kim, S.-C. Analysis of Shielding Performance of Radiation-Shielding Materials According to Particle Size and Clustering Effects. *Appl. Sci.* **2021**, *11*, 4010. [CrossRef]
33. Fakhoury, E.; Provencher, J.-A.; Subramaniam, R.; Finlay, D.J. Not all lightweight lead aprons and thyroid shields are alike. *J. Vasc. Surg.* **2018**, *70*, 246–250. [CrossRef] [PubMed]
34. Hertault, A. Shields Up! How Much Should You Rely on Your Lightweight Garments? *Eur. J. Vasc. Endovasc. Surg.* **2019**, *57*, 740. [CrossRef] [PubMed]
35. Lu, H.; Boyd, C.; Dawson, J. Lightweight Lead Aprons: The Emperor's New Clothes in the Angiography Suite? *Eur. J. Vasc. Endovasc. Surg.* **2019**, *57*, 730–739. [CrossRef]
36. Kim, S.-C.; Cho, S.-H. Analysis of the Correlation between Shielding Material Blending Characteristics and Porosity for Radiation Shielding Films. *Appl. Sci.* **2019**, *9*, 1765. [CrossRef]
37. Pianpanit, T.; Saenboonruang, K. High-Energy Photon Attenuation Properties of Lead-Free and Self-Healing Poly (Vinyl Alcohol) (PVA) Hydrogels: Numerical Determination and Simulation. *Gels* **2022**, *8*, 197. [CrossRef] [PubMed]
38. Elsafi, M.; El-Nahal, M.A.; Sayyed, M.I.; Saleh, I.H.; Abbas, M.I. Novel 3-D printed radiation shielding materials embedded with bulk and nanoparticles of bismuth. *Sci. Rep.* **2022**, *12*, 12467. [CrossRef]
39. Kaewpirom, S.; Chousangsuntorn, K.; Boonsang, S. Evaluation of Micro- and Nano-Bismuth(III) Oxide Coated fabric for Environmentally Friendly X-Ray Shielding Materials. *ACS Omega* **2022**, *7*, 28248–28257. [CrossRef]
40. El-Khatib, A.M.; Shalaby, T.I.; Antar, A.; Elsafi, M. Experimental Study of Polypropylene with Additives of Bi_2O_3 Nanoparticles as Radiation-Shielding Materials. *Polymer* **2022**, *14*, 2253. [CrossRef]
41. Tiamduangtawan, P.; Kamkaew, C.; Kuntonwatchara, S.; Wimolmala, E.; Saenboonruang, K. Comparative mechanical, self-healing, and gamma attenuation properties of PVA hydrogels containing either nano- or micro-sized Bi_2O_3 for use as gamma-shielding materials. *Radiat. Phys. Chem.* **2020**, *177*, 109164. [CrossRef]
42. Winter, H.; Brown, A.L.; Goforth, A.M. Bismuth-Based Nano- and Microparticles in X-Ray Contrast, Radiation Therapy, and Radiation Shielding Applications. In *Bismuth—Advanced Applications and Defects Characterization*; Zhou, Y., Dong, F., Jin, S., Eds.; InterOpen: London, UK, 2018; Chapter 4, ISBN 978-1-78923-263-9. [CrossRef]
43. Wang, B.; Ting, C.-Y.; Lai, C.-S.; Tsai, Y.-S. Bismuth Pelvic X-Ray Shielding Reduces Radiation Dose Exposure in Pediatric Radiography. *Hindawi BioMed Res. Int.* **2021**, *2021*, 9985714. [CrossRef]
44. Cadavid, D.A.R.; Layman, R.R.; Nishino, T.; Slutzky, J.L.; Li, Z.; Cornish, K. Guayule Natural Rubber Latex and Bi_2O_3 Films for X-ray Attenuating Medical Gloves. *Materials* **2022**, *15*, 1184. [CrossRef] [PubMed]
45. Alshahri, S.; Alsuhybani, M.; Alosime, E.; Almurayshid, M.; Alrwais, A.; Alotaibi, S. LDPE/Bismuth Oxide Nanocomposite: Preparation, Characterization and Application in X-ray Shielding. *Polymers* **2021**, *13*, 3081. [CrossRef] [PubMed]
46. Poltabtim, W.; Wimolmala, E.; Markpin, T.; Sombatsompop, N.; Rosarpitak, V.; Saenboonruang, K. X-ray Shielding, Mechanical, Physical, and Water Absorption Properties of Wood/PVC Composites Containing Bismuth Oxide. *Polymers* **2021**, *13*, 2212. [CrossRef] [PubMed]
47. Thumwong, A.; Chinnawet, M.; Intarasena, P.; Rattanapongs, C.; Tokonami, S.; Ishikawa, T.; Saenboonruang, K. A Comparative Study on X-ray Shielding and Mechanical Properties of Natural Rubber Latex Nanocomposites Containing Bi_2O_3 or $BaSO_4$: Experimental and Numerical Determination. *Polymers* **2022**, *14*, 3654. [CrossRef] [PubMed]

48. Seenappa, L.; Manjunatha, H.; Chandrika, B.; Chikka, H. A Study of Shielding Properties of X-ray and Gamma in Barium Compounds. *J. Radiat. Prot. Res.* **2017**, *42*, 26–32. [CrossRef]
49. Kim, S.-C.; Dong, K.-R.; Chung, W.-K. Medical radiation shielding effect by composition of barium compounds. *Ann. Nucl. Energy* **2012**, *47*, 1–5. [CrossRef]
50. Issa, S.A.; Zakaly, H.M.; Pyshkina, M.; Mostafa, M.Y.; Rashad, M.; Soliman, T. Structure, optical, and radiation shielding properties of PVA–$BaTiO_3$ nanocomposite films: An experimental investigation. *Radiat. Phys. Chem.* **2020**, *180*, 109281. [CrossRef]
51. Hong, J.W.; Kim, D.H.; Kim, S.W.; Choi, S.H.; Lee, G.-E.; Seo, H.-K.; Kim, S.-H.; Lee, Y. Effectiveness evaluation of self-produced micro- and nanosized tungsten materials for radiation shielding with diagnostic X-ray imaging system. *Optik* **2018**, *172*, 760–765. [CrossRef]
52. Al-Ghamdi, H.; Hemily, H.M.; Saleh, I.H.; Ghataas, Z.F.; Abdel-Halim, A.A.; Sayyed, M.I.; Yasmin, S.; Almuqrin, A.H.; Elsafi, M. Impact of WO_3-Nanoparticles on Silicone Rubber for Radiation Protection Efficiency. *Materials* **2022**, *15*, 5706. [CrossRef]
53. Aghaz, A.; Faghihi, R.; Mortazavi, S.; Haghparast, A.; Mehdizadeh, S.; Sina, S. Radiation Attenuation Properties of Shielding Materials Containing Micro and Nano-sized WO3 in Diagnostic X-ray Energy Range. *Int. J. Radiat. Res.* **2016**, *14*, 127–131. [CrossRef]
54. Azman, N.N.; Siddiqui, S.; Hart, R.; Low, I. Effect of particle size, filler loadings and x-ray tube voltage on the transmitted x-ray transmission in tungsten oxide—Epoxy composites. *Appl. Radiat. Isot.* **2012**, *71*, 62–67. [CrossRef] [PubMed]
55. Hashemi, S.A.; Mousavi, S.M.; Faghihi, R.; Arjmand, M.; Rahsepar, M.; Bahrani, S.; Ramakrishna, S.; Lai, C.W. Superior X-ray Radiation Shielding Effectiveness of Biocompatible Polyaniline Reinforced with Hybrid Graphene Oxide-Iron Tungsten Nitride Flakes. *Polymers* **2020**, *12*, 1407. [CrossRef] [PubMed]
56. Kijima, K.; Monzen, H.; Matsumoto, K.; Tamura, M.; Nishimura, Y. The Shielding Ability of Novel Tungsten Rubber Against the Electron Beam for Clinical Use in Radiation Therapy. *Anticancer. Res.* **2018**, *38*, 3919–3927. [CrossRef] [PubMed]
57. Dejangah, M.; Ghojavand, M.; Poursalehi, R.; Gholipour, P.R. X-ray attenuation and mechanical properties of tungsten-silicone rubber nanocomposites. *Mater. Res. Express* **2019**, *6*, 085045. [CrossRef]
58. Yonphan, S.; Chaiphaksa, W.; Kalkornsurapranee, E.; Tuljittraporn, A.; Kothan, S.; Kaewjaeng, S.; Intachai, N.; Wongdamnern, N.; Kedkaew, C.; Kim, H.; et al. Development of flexible radiation shielding materials from natural Rubber/Sb_2O_3 composites. *Radiat. Phys. Chem.* **2022**, *200*, 110379. [CrossRef]
59. Zarei, M.; Sina, S.; Hashemi, S.A. Superior X-ray radiation shielding of biocompatible platform based on reinforced polyaniline by decorated graphene oxide with interconnected tungsten–bismuth–tin complex. *Radiat. Phys. Chem.* **2021**, *188*, 109588. [CrossRef]
60. Uthoff, H.; Benenati, M.J.; Katzen, B.T.; Peña, C.; Gandhi, R.; Staub, D.; Schernthaner, M. Lightweight Bilayer Barium Sulfate–Bismuth Oxide Composite Thyroid Collars for Superior Radiation Protection in Fluoroscopy-guided Interventions: A Prospective Randomized Controlled Trial. *Radiology* **2014**, *270*, 601–606. [CrossRef]
61. Johansen, S.; Hauge, I.H.R.; Hogg, P.; England, A.; Lança, L.; Gunn, C.; Sanderud, A. Are Antimony-Bismuth Aprons as Efficient as Lead Rubber Aprons in Providing Shielding against Scattered Radiation? *J. Med. Imaging Radiat. Sci.* **2018**, *49*, 201–206. [CrossRef]
62. Kim, S.-C. Development of a Lightweight Tungsten Shielding Fiber That Can Be Used for Improving the Performance of Medical Radiation Shields. *Appl. Sci.* **2021**, *11*, 6475. [CrossRef]
63. Kim, S.-C. Construction of a Medical Radiation-Shielding Environment by Analyzing the Weaving Characteristics and Shielding Performance of Shielding Fibers Using X-ray-Impermeable Materials. *Appl. Sci.* **2021**, *11*, 1705. [CrossRef]
64. Kim, S.-C.; Son, J.-S. Manufacturing and performance evaluation of medical radiation shielding fiber with plasma thermal spray coating technology. *Sci. Rep.* **2021**, *11*, 22418. [CrossRef] [PubMed]
65. Mirzaei, M.; Zarrebini, M.; Shirani, A.; Shanbeh, M.; Borhani, S. X-ray shielding behavior of garment woven with melt-spun polypropylene monofilament. *Powder Technol.* **2018**, *345*, 15–25. [CrossRef]
66. Mirzaei, M.; Zarrebini, M.; Shirani, A.; Shanbeh, M.; Borhani, S. X-ray shielding by a novel garment woven with melt-spun monofilament weft yarn containing lead and tin particles. *Text. Res. J.* **2017**, *89*, 63–75. [CrossRef]
67. Liang, D.; Shen, F.; Bao, Z.; Liu, Y.; Li, H. Research on textile materials for X-ray shielding. *E3S Web Conf.* **2021**, *290*, 01013. [CrossRef]
68. Aral, N.; Nergis, F.B.; Candan, C. An alternative X-ray shielding material based on coated textiles. *Text. Res. J.* **2015**, *86*, 803–811. [CrossRef]
69. Verma, S.; Mili, M.; Sharma, C.; Bajpai, H.; Pal, K.; Qureshi, D.; Hashmi, S.A.R.; Srivastava, A.K. Advanced X-ray shielding and antibacterial smart multipurpose fabric impregnated with polygonal shaped bismuth oxide nanoparticles in carbon nanotubes via green synthesis. *Green Chem. Lett. Rev.* **2021**, *14*, 272–285. [CrossRef]
70. Wang, Y.; Ding, P.; Xu, H.; Li, Q.; Guo, J.; Liao, X.; Shi, B. Advanced X-ray Shielding Materials Enabled by the Coordination of Well-Dispersed High Atomic Number Elements in Natural Leather. *ACS Appl. Mater. Interfaces* **2020**, *12*, 19916–19926. [CrossRef]
71. Dehghan, N.; Movahedi, M.; Abdi, A.; Mehdizadeh, A.; Heidari, E.; Masumi, Y.; Abbaszadeh, M. Novel paint design based on nanopowder to protection against X and gamma rays. *Indian J. Nucl. Med.* **2014**, *29*, 18–21. [CrossRef]
72. Schmid, E.; Panzer, W.; Schlattl, H.; Eder, H. Emission of fluorescent x-radiation from non-lead based shielding materials of protective clothing: A radiobiological problem? *J. Radiol. Prot.* **2012**, *32*, N129–N139. [CrossRef]
73. Schlattl, H.; Zankl, M.; Eder, H.; Hoeschen, C. Shielding properties of lead-free protective clothing and their impact on radiation doses. *Med. Phys.* **2007**, *34*, 4270–4280. [CrossRef]

74. Eder, H.; Schlattl, H. IEC 61331-1: A new setup for testing lead free X-ray protective clothing. *Phys. Medica* **2018**, *45*, 6–11. [CrossRef]
75. Eder, H.; Panzer, W.; Schöfer, H. Is the lead equivalent suitable for assessing the protective effect of lead-free X-ray protective clothing? *Rofo* **2005**, *177*, 399–404. [CrossRef] [PubMed]
76. Schöpf, T.; Pichler, T. Radiation Protection Clothing in X-Ray Diagnostics—Influence of the Different Methods of Measurement on the Lead Equivalent and the Required Mass. *Rofo* **2016**, *188*, 768–775. [CrossRef] [PubMed]
77. Jones, A.K.; Wagner, L.K. On the (f)utility of measuring the lead equivalence of protective garments. *Med. Phys.* **2013**, *40*, 063902. [CrossRef]
78. Büermann, L. Determination of lead equivalent values according to IEC 61331-1:2014—Report and short guidelines for testing laboratories. *J. Instrum.* **2016**, *11*, T09002. [CrossRef]
79. McCaffrey, J.P.; Shen, H.; Downton, B.; Mainegra-Hing, E. Radiation attenuation by lead and nonlead materials used in radiation shielding garments. *Med. Phys.* **2007**, *34*, 530–537. [CrossRef] [PubMed]